Universitat Autònoma de Barcelona

Dipòsit digital de documents de la UAB

This is the **accepted version** of the journal article:

Álvarez Prada, Luis Ignacio; Peral, Daniel; Song, Mary; [et al.]. «Ruthenium nanoparticles supported on carbon-based nanoallotropes as co-catalyst to enhance the photocatalytic hydrogen evolution activity of carbon nitride». Renewable Energy, Vol. 168 (May 2021), p. 668-675. DOI 10.1016/j.renene.2020.12.070

This version is available at https://ddd.uab.cat/record/288228

under the terms of the BY-NC-ND license

Ruthenium Nanoparticles Supported on Carbon-based Nanoallotropes as Co-catalyst to Enhance the Photocatalytic Hydrogen Evolution Activity of Carbon Nitride

Ignacio Álvarez-Prada,[a] Daniel Peral,[b] Mary Song,[b] Jose Muñoz,[c*] Nuria Romero,[a] Lluís Escriche,[a] Amitava Acharjya,[d] Arne Thomas,[d] Reinhard Schomäcker,[b] Michael Schwarze,[b] Xavier Sala,[a*] Minoo Tasbihi,[b*] Jordi García-Antón[a*]

[a] Departament de Química, Unitat de Química Inorgànica, Universitat Autònoma de Barcelona, 08193-Bellaterra, Barcelona, Spain. E-mails: Xavier.Sala@uab.cat; Jordi.GarciaAnton@uab.es

[b] Department of Chemistry, Technische Universität Berlin, 10623 Berlin, Germany. E-mail: minoo.tasbihi@tu-berlin.de

[c] Institut de Ciència de Materials de Barcelona (ICMAB-CSIC), Campus UAB, 08193 Bellaterra, Barcelona, Spain. E-mail: jmunoz@icmab.es

[d] Institute of Chemistry: Functional Materials, Technische Universität Berlin, 10623 Berlin, Germany.

Abstract

Development of competent and cost-effective materials for hydrogen evolution reaction (HER) has been attracting great attention since hydrogen is hailed as a promising environmentally friendly energy source to reduce the greenhouse emissions. Herein, Ru(0) nanoparticles (RuNPs) have been stabilized onto the surface of four different conducting carbon nanomaterials (CNMs) from 0D to 3D, such as 0D carbon nanohorns (CNH), 1D single-walled carbon nanotubes (CNTs), 2D reduced graphene oxide (rGO) and 3D graphite (GP), for their use in the photocatalytic HER. For this aim, the resulting RuNP@CNMs where physically mixed with mesoporous graphitic carbon nitride (mpg-CN) in an optimum composition ratio to maximize the photocatalytic HER activity. Notably, the resulting four hybrid RuNPs@CNM/mpg-CN materials showed an outstanding increase in the hydrogen evolution reaction (HER) when compared with the pristine mesoporous graphitic carbon nitride without co-catalyst. A comparison on the photocatalytic activity of the four hybrid RuNPs@CNMs physically mixed with mpg-CN and a deep study on the fate of the nanohybrids after catalysis are presented.

Keywords: Hydrogen / hydrogen evolution reaction / ruthenium / carbon nitride / photocatalysis

1. Introduction

The storing of solar energy into the chemical bonds of H_2, through the so-called artificial photosynthesis, and its use as a solar fuel, is of major interest to achieve in the future an environmentally sustainable energy supply [1].

Many efforts are currently devoted to improving the light-driven water splitting into molecular H_2 and O_2 [2,3]. Water splitting can be divided into two half-reactions, namely the oxygen evolution reaction (OER) and hydrogen evolution reaction (HER). To achieve this, first of all, a photoactive material able to harvest sunlight is needed. Several semiconducting materials are suitable, if they exhibit appropriate band gaps [4]. In these cases, photons from the light source can excite electrons from the valence band (VB) to the conduction band (CB) of the semiconductor (SC), which will then be used to reduce protons to H_2. In doing so, holes are generated in the SC valence band that will subsequently oxidize water to O_2. However, suitable co-catalysts are required to improve the rate of the reactions and minimize the recombination of the excited electrons and holes.

Platinum nanoparticles (PtNPs) have been extensively used as co-catalysts in HER reactions since they display the highest efficiencies with minimum overpotentials in acidic media [5]. However, platinum scarcity and high cost, together with its low stability (corrosion) in basic media has prompted the scientific community to search for other co-catalysts for the HER reaction, from molecular [6,7] to colloidal and more expanded solid catalysts [8]. In this respect, several distinguished and attractive properties are associated to the use of colloidal (photo)electrocatalysts when compared with molecular systems [9]. Generally, colloidal systems exhibit high stability and activity due to the large number of colloidal units that can be deposited onto the surface of the electrode / photoactive semiconducting material.

Ruthenium nanoparticles (RuNPs) can be an alternative for the replacement of platinum as co-catalyst in the HER reaction [10]. Recently, several studies highlighted the competitive intrinsic activity of RuNPs as HER co-catalysts and their higher stability (vs. benchmark PtNPs) under alkaline conditions [11,12]. Additionally, Ru is at least six times cheaper than Pt. Despite their sound performance as electrocatalysts, the use of RuNPs in visible light driven HER photocatalytic systems has been hindered by the inefficient transfer of electrons from the photosensitive molecule or material to the RuNPs [13]. To bypass this

problem, the use of a photosensitizer (e.g. $[Ru(bpy)_3]^{2+}$) in combination with an electron mediator (e.g. methyl viologen) is a common strategy [13]. If the photosensitizer (e.g. 2-phenyl-4-(1-naphthyl)-quinolinium ion, $QuPh^+$-NA) is able to attain long-lived charge-separated states after photoexcitation, the use of an electron mediator can be bypassed [14,15,16], attaining high H_2 production rates for short reaction times under UV-vis irradiation (λ > 340 nm) and mixed MeCN:H_2O media.

Surface environment, size, shape, structure and homogeneity of the nanoparticulated co-catalysts in photocatalytic systems are key characteristics for their activity and stability. Therefore, it is essential to use a reproducible synthetic method of nanoparticles that controls these characteristics. The so-called organometallic approach allows to reproducibly obtain small nanoparticles homogeneous in size using mild reaction conditions and with controlled surface environment [17,18]. These well characterized materials permit to correlate the physical/chemical properties of the system and its catalytic output, allowing to rationally design new enhanced catalytic systems. In this context, we have recently reported two Ru-based nanocatalysts prepared by the organometallic approach with outstanding performances in electrocatalytic HER [19,20,21]

Herein, we report the application of RuNPs as co-catalysts with the organic semiconductor mesoporous graphitic carbon nitride (mpg-CN). As observed in the literature with other systems based on graphitic carbon nitride (g-CN) [22,23,24] while the use of pure g-CN for the HER reaction produces low amounts of H_2, the activity increases substantially when coupled with the appropriate co-catalyst [25,26,27].

2. Results and Discussion

2.1. Synthesis and characterization of RuNP@CNMs

Four different CNMs, including 0D carbon nanohorns (CNHs), 1D carbon nanotubes (CNTs), 2D reduced graphene oxide (rGO) and 3D graphite (GP) have been used as nanotemplates to stabilize RuNPs by the previously described organometallic approach [17,18]. The synthesis of the RuNPs was carried out in a Fisher-Porter reactor by hydrogenation (2h, 3 bar) of the organometallic precursor [Ru(cod)(cot)] (cod = 1,5-cyclooctadiene; cot = 1,3,5-cyclooctatriene) dissolved in THF in the presence of the chosen carbon support (Scheme 1). The obtained hybrid materials (RuNPs@CNH, RuNPs@CNT, RuNPs@rGO and RuNPs@GP) have been characterized by transmission electron microscopy (TEM), X-ray photoelectron spectroscopy (XPS) and inductively coupled plasma optical emission spectrometry (ICP-OES) before their use as co-catalysts in the photocatalytic water splitting reaction.

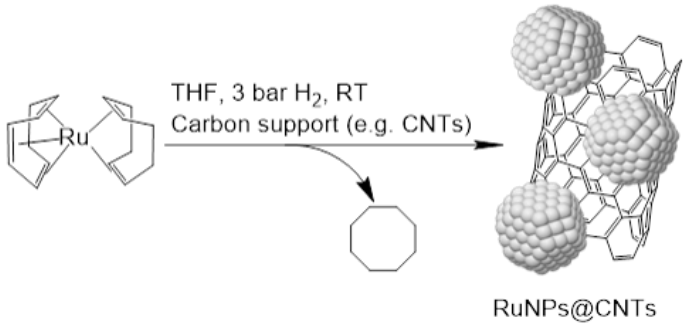

Scheme 1. Synthesis of RuNP@CNMs using RuNP@CNTs for exemplification.

TEM analyses of the four hybrid systems confirm the presence of small nanoparticles onto the surface of the CNMs (Figure 1). In the case of CNHs and CNTs, the surface is partially covered by isolated NPs. Regarding to rGO and GP, the surface is totally covered by the NPs, being even partially agglomerated. This behaviour can be due to the fact that, for the same amount of CNM, the total surface area for 0D (CNHs) or 1D (CNTs) materials is higher than for 2D (rGO) or 3D (GP) materials. The mean size of the RuNPs is between 1.3 and 2.3 nm, and the size of the RuNPs is in the following order for the different carbon supports: CNHs (1.3 nm) < rGO (1.5 nm) < GP (2.0 nm) < CNTs (2.3 nm). Although the sizes do not differ much, the NPs might be affected by the nature of the carbon support.

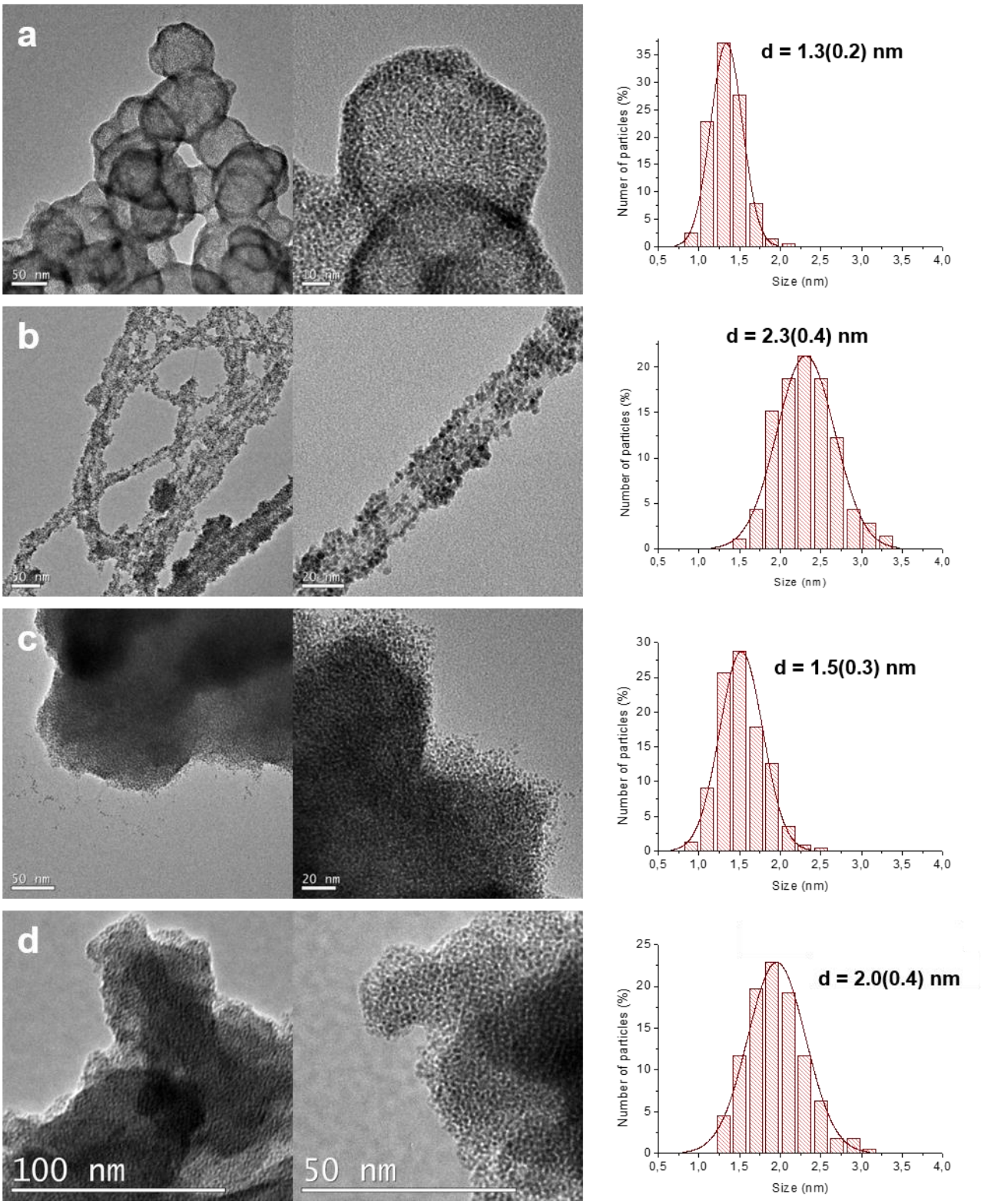

Figure 1. TEM images and size distribution of Ru nanoparticles supported on CNHs (a), CNTs (b), rGO (c) and GP (d).

For a better understanding of the chemical composition of the NPs, XPS measurements have been recorded. As shown in Figure S1, two Ru species can be

encountered, metallic Ru^0 (Ru $3d_{5/2}$ peaks centred at 279.8 eV, Ru $3d_{3/2}$ peaks centred at 284.0 eV) and Ru^{IV} (Ru $3d_{5/2}$ peaks centred at 280.8 eV, Ru $3d_{3/2}$ peaks centred at 285.0 eV). The presence of Ru^{IV} can be attributed to the partial oxidation of the Ru^0 NPs at the surface when exposed to air. This behaviour has been previously observed for other RuNPs prepared by the organometallic approach [20,28]. In the previous cases, it has been observed that non-supported RuNPs burn when abruptly exposed to air but are protected by a thin RuO_2 surface layer under controlled (slow) air exposition. In our case, the reductive properties of CNMs would be also responsible of preventing the full oxidation of the RuNPs. Peaks attributable to C can be also seen in XPS spectra. These peaks, found between 284.0 and 290.3 eV, can be ascribed to aliphatic, aromatic and partially oxidized carbon atoms.

The actual amount of Ru loading of the hybrid materials was measured by inductively coupled plasma-optical emission spectroscopy (ICP-OES; wt.%) analyses, giving 42% (RuNPs@CNH), 41% (RuNPs@CNT), 37% (RuNPs@rGO) and 32% (RuNPS@GP) of Ru. Interestingly, a general increase of the loading of the RuNPs with the increase of the surface to volume ratio of the CNMs can be observed.

2.2. Photocatalytic Tests

The four different RuNPs@CNM samples have been used as co-catalysts to improve the activity of mpg-CN in the photocatalytic HER. The preparation of RuNPs@CNM/mpg-CN has been accomplished by physically mixing both materials with a mortar. Scanning Electron Microscopy-Field Emission Gun (SEM-FEG), Energy-Dispersive X-ray spectroscopy (EDX), specific surface area (S_{BET}) and powder X-ray diffraction (XRD) experiments have been performed for RuNPs@CNH/mpg-CN, RuNPs@CNT/mpg-CN, RuNPs@rGO/mpg-CN and RuNPs@GP/mpg-CN. In all cases (Figures S2-S5), SEM-FEG micrographs show the presence of big (> 1 μm) mpg-CN particles partially covered by the corresponding RuNPs@CNM nanohybrids. RuNPs@CNM appears as white dots due to the use of a backscattered-electrons detector and are embedded onto darker mpg-CN particles. EDX spectra (Figures S2-S5) confirm the presence of Ru in the RuNPs@CNM/mpg-CN nanohybrids.

Specific surface areas (S_{BET}) have been measured in order to find out any possible changes in the structural features of mpg-CN samples (BET isotherms and related data can be found in Figure S6 and Table S1). Pure mpg-CN displays a specific surface area of 134.3 m^2/g. However, after RuNPs@CNM loading, the specific surface areas of the RuNPs@CNM/mpg-CN samples significantly decrease. This behaviour can be attributed to the partial blocking of the mpg-CN mesopores after RuNPs@CNM loading. The decline in the specific surface area is more pronounced when the RuNPs@CNM loading increases. In this way, for RuNPs@CNT/mpg-CN with a loading of 0.16 mg of RuNPs@CNT (0.64 μmol of Ru) in 25 mg of mpg-CN, S_{BET} decreases to 83.1 m^2/g and for a loading of 0.39 mg of RuNPs@CNT (1.60 μmol of Ru) in 25 mg of mpg-CN, S_{BET} further decreases up to 49.7 m^2/g.

If the four different CNM are considered, with a loading of ca. 1.60 μmol of Ru, the specific surface area is similar for CNHs (51.8 m^2/g), CNTs (49.7 m^2/g) and rGO (51.4 m^2/g). The S_{BET} value for GP, 70.4 m^2/g, indicates that the bigger particles of GP are blocking the mpg-CN mesopores to a lesser extent.

Powder X-ray diffraction (XRD) patterns of RuNPs@CNM/mpg-CN photocatalysts with a loading of ca. 0.63 μmol of Ru have been recorded and compared to that of pure mpg-CN (Figure 2). All the diffractograms display two peaks at 2θ values of 13.1˚ and 27.4˚, showing that the crystallinity of the mpg-CN is preserved after Ru loading. Reflection at 2θ value of 27.4˚ can be attributed to the layered stacking and reflection at 13.1˚ indicates inter planar repetition of tris-triazine units [29]. Due to the low Ru loading, no reflections corresponding to the metallic nanoparticles have been detected.

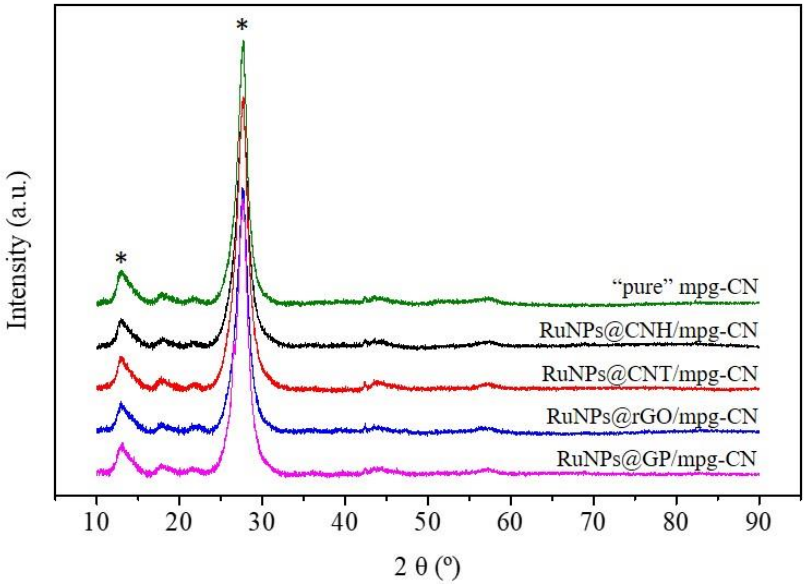

Figure 2. XRD patterns of the photocatalysts. * mpg-CN.

Initial photocatalytic tests were performed to obtain the best ratio of the single components in a RuNPs@CNH/mpg-CN hybrid sample (Figure 3, Table 1). The experiments were performed under visible light irradiation (>395 nm; 4 hrs) using a 300 W Xe lamp in a screening quartz glass reactor with planar irradiation area (Figure S7). The amount of H_2 generated after photocatalysis was measured by gas chromatography (GC) from headspace samples. It is worth noting that the amount of H_2 produced was practically negligible using pure mpg-CN, mpg-CN or mpg-CN mixed with CNHs (Figure 3, Table 1, entries 1, 2 and 3).

Table 1. Photocatalytic H_2 production in the screening reactor from different amounts of RuNPs@CNH under visible light irradiation (>395 nm; 4 hrs) using a 300 W Xe lamp and TEOA as the sacrificial electron donor. [a] Only CNHs. [b] µmol of H_2 production per h and per g of catalyst (mpg-CN + RuNPs@CNM). [c] TON and TOF considering total molar amount of Ru, after 4 hrs.

Entry	mpg-CN (mg)	RuNPs@CNH (mg)	Ru (µmol)	H_2 (µmol)	H_2 evol. rate (µmol·h^{-1}·g^{-1})[b]	TON[c] (-)	TOF[c] (h^{-1})
1	26.3	-	–	1.6	17	–	–
2	-	1.62	6.75	-	-	–	–
3	26.3	1.51[a]	–	0.5	5	–	–
4	26.3	0.16	0.68	36.2	340	53	13.3
5	26.3	0.41	1.69	41.0	420	24	6.1
6	26.3	0.81	3.38	31.9	324	9	2.4
7	26.3	1.62	6.75	10.6	105	2	0.4

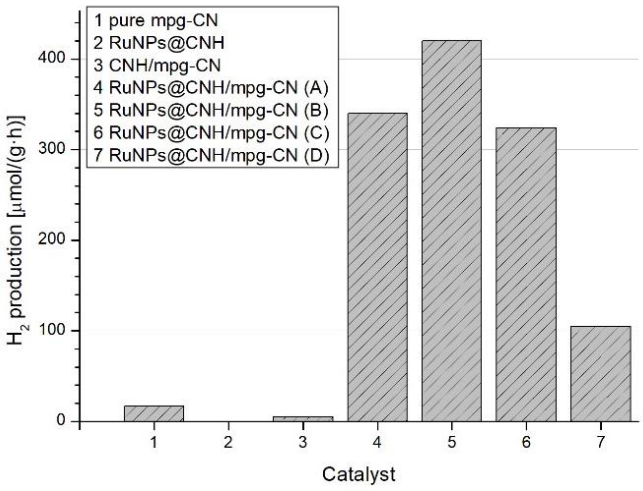

Figure 3. Photocatalytic H_2 evolution using different loadings of RuNPs@CNH in mpg-CN under visible light irradiation (>395 nm; 4 hrs) using 300 W Xe lamp. Ru loadings: A = 0.68 µmol; B = 1.69 µmol; C = 3.38 µmol; D = 6.75 µmol.

The best results for photocatalytic H_2 evolution were obtained when using the two lowest loadings of Ru on the CNHs as carbon nanotemplates (36.2 and 41.0 µmol of H_2 produced from 0.68 and 1.69 µmol of Ru, Table 1, entries 4 and 5, respectively). This can be explained since for higher loadings (3.38 and 6.75 µmol of Ru, Table 1, entries 6 and 7, respectively) more light is absorbed by the black RuNPs@CNH hybrid material, preventing light from reaching the surface of the photocatalytic active mpg-CN and therefore, decreasing the photogenerated amount of H_2. Figure S8 shows the increasing darkening of the hybrid materials when the amount of RuNPs@CNH increases. The highest amount of H_2 was produced using a loading of 1.69 µmol of Ru (41.0 µmol of H_2 produced, TON 24, TOF 6.1, entry 5), which presents an optimum of the number of active sites with low light absorption of the RuNP@CNH. Nevertheless, the highest TON / TOF values, and therefore the fastest photocatalytic reaction, were obtained using 0.68 µmol of Ru (36.2 µmol of H_2, TON 53, TOF 13.3 h^{-1}, Table 1, entry 4). Hence, photocatalytic experiments were performed in the standard reactor showed in Figures S9 and S10 using 0.68 and 1.69 µmol of Ru loadings for the RuNPs@CNH/mpg-CN, RuNPs@CNT/mpg-CN, RuNPs@rGO/mpg-CN and RuNPS@GP/mpg-CN hybrid materials in the presence of visible light irradiation (>395 nm) from a 300W Xe lamp (24 hours irradiation) using TEOA as the sacrificial electron donor. The experimental data can be gathered in Table 2. The amount of H_2 produced ($\mu mol \cdot h^{-1} \cdot g^{-1}$) has been measured from the slope of the

curves of mol of H_2 vs. time (Figure S11) and confirmed by GC-MS. The TON values per Ru for the two concentrations used were calculated and plotted in Figure 4, together with the values of H_2 produced ($\mu mol \cdot h^{-1} \cdot g^{-1}$).

Table 2. Photocatalytic H_2 evolution in the standard reactor using different loadings of RuNPs@CNM in mpg-CN under visible light irradiation (>395 nm; 24 hrs) using 300 W Xe lamp and TEOA as the sacrificial electron donor. 25 mg mpg-CN and the corresponding mg RuNPs@CNH in 38 mL of TEOA 10%. [a] µmol of H_2 production per h and per g of catalyst (mpg-CN + RuNPs@CNM) [b] TON and TOF considering total molar amount of Ru after 24 hrs.

Entry	Hybrid Material	RuNPs@CNM (mg)	Ru (µmol)	H_2 evol. rate ($\mu mol \cdot h^{-1} \cdot g^{-1}$)[a]	H_2 (µmol)	TON[b] (-)	TOF[b] (h^{-1})
1	mpg-CN	–	–	2.0	1.2	–	–
2	RuNPs@CNH/mpg-CN (b)	0.15	0.63	67.4	40.1	64	2.7
3	RuNPs@CNH/mpg-CN (a)	0.39	1.62	168.3	101.3	63	2.6
4	RuNPs@CNT/mpg-CN (b)	0.16	0.64	120.6	72.5	113	4.7
5	RuNPs@CNT/mpg-CN (a)	0.39	1.60	197.4	118.0	74	3.1
6	RuNPs@rGO/mpg-CN (b)	0.18	0.64	73.8	44.3	69	2.9
7	RuNPs@rGO/mpg-CN (a)	0.44	1.60	146.5	87.4	55	2.3
8	RuNPs@GP/mpg-CN (b)	0.21	0.65	108.2	65.1	100	4.2
9	RuNPs@GP/mpg-CN (a)	0.51	1.60	186.6	112.9	70	2.9

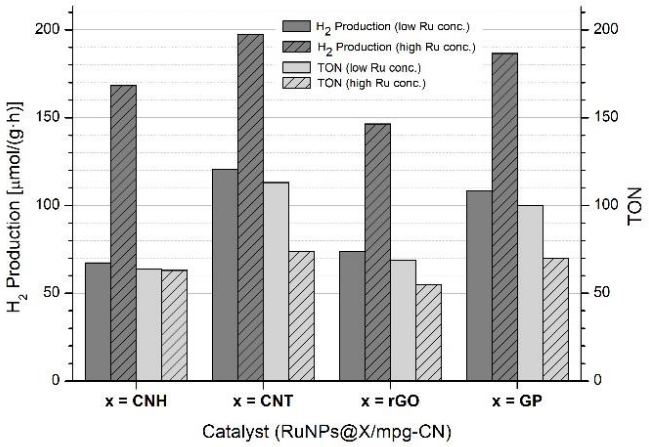

Figure 4. Photocatalytic H_2 production and TON using different loadings of RuNPs@CNM in mpg-CN under visible light irradiation (>395 nm; 24 hrs) using 300 W Xe lamp. TON considering total µmol Ru. Ru loading: 0.68 µmol of Ru for low Ru conc. and 1.69 µmol of Ru for high Ru conc.

In all cases, higher amount of H_2 has been produced using higher loadings of Ru (Table 2, entries 3, 5, 7 and 9), in agreement with those results obtained from the initial tests, performed with RuNPs@CNH for 4 h, where the highest amount of H_2 was obtained with 1.69 µmol of Ru (Table 1, entry 5).

Thus, for the standard reactor, the best results have been obtained using RuNPs@CNT/mpg-CN with 118.0 µmol of H_2 production in 24 hrs (Table 2, entry

5) and with RuNPs@GP/mpg-CN, which generates 112.9 μmol of H_2 (Table 2, entry 9). Nevertheless, the catalyst with the lowest performance using the same Ru loading (87.4 μmol of H_2 production by RuNPs@rGP/mpg-CN, Table 2, entry 7) produced only 25% less H_2 than RuNPs@CNT/mpg-CN, meaning that the nature of the carbon support is not crucial for the activity of the catalysts, but the CNM itself is crucial for the stabilization of the Ru NPs.

Considering the photocatalytic activity of the samples containing the same carbonaceous support, higher TON / TOF numbers are obtained for the samples with lower loadings of Ru (Table 2, entries 2, 4, 6 and 8). The highest photocatalytic activity is obtained again for RuNPs@CNT/mpg-CN with the lower Ru loading, with TON / TOF values of 113 and 4.7 h^{-1}, respectively (Table 2, entry 4). This trend can be explained as a compromise between the amount of Ru co-catalyst and the darkening produced on the whole RuNPs@CNM/mpg-CN catalyst. All in all, the hybrid materials in the present study are thus one of the few examples in the literature where a photoactive material is able to efficiently carry out the electron-transfer process with Ru NPs for the photocatalytic HER reaction with visible light and in absence of an electron mediator.

The main photocatalytic data of RuNPs@CNM/mpg-CN and those of examples in the literature based on carbon nitride-supported nanocatalysts are shown in Table S2. To the best of our knowledge, this is the first time in which Ru nanoparticles are supported onto carbon nitride and applied in HER. Literature reports consist of carbon nitride-supported Pt (most of the examples), Pd and Ni nanoparticles and their corresponding alloys with Co, and Au. Archetypal Pt-based photocatalysts display superior HER activities, while the supported Ru-based systems reported in this work outperform Ni-based photocatalysts (compare entries 1-4 vs. entries 15-16, Table S2).

The fate of the catalyst after the photocatalytic experiments were studied by TEM and XPS. Due to the low loading of RuNPs@CNMs in mpg-CN, TEM analyses after the photocatalytic experiments have been performed with the hybrid systems with a higher content of Ru. RuNPs can be observed for all four hybrid materials (Figure S12 in Supporting Information), with similar size and shape as those observed before the photocatalytic experiments. This behaviour is in agreement with the data obtained for the photocatalytic H_2 evolution experiments, where no deactivation is observed after 24 hrs of visible light irradiation (Figure S11).

XPS analyses after the photocatalytic experiments (Figure S13 in Supporting Information) demonstrate the presence of two Ru phases for all RuNPs@CNM/mpg-CN hybrid samples: metallic Ru^0 ($Ru\ 3d_{5/2}$ peaks centred at 279.8 eV, $Ru\ 3d_{3/2}$ peaks centred at 284.0 eV) and Ru^{IV} ($Ru\ 3d_{5/2}$ peaks centred at 280.8 eV, $Ru\ 3d_{3/2}$ peaks centred at 285.0 eV). During the photocatalytic experiments, the samples are exposed to a reducing ambiance (presence of TEOA and H_2 formed) that helps to maintain the initial Ru^0 / RuO_2 duality of the RuNPs. In order to prove the stability of the photocatalytic systems, a long-term experiment was carried out with RuNPs@CNT@mpg-CN (Ru loading = 1.60 µmol) under the same experimental conditions as those described in Table 2 but for 75 hrs. Figure 5 shows the photocatalytic H_2 evolution for this experiment, where no sign of deactivation can be detected, and proves the high stability of the system.

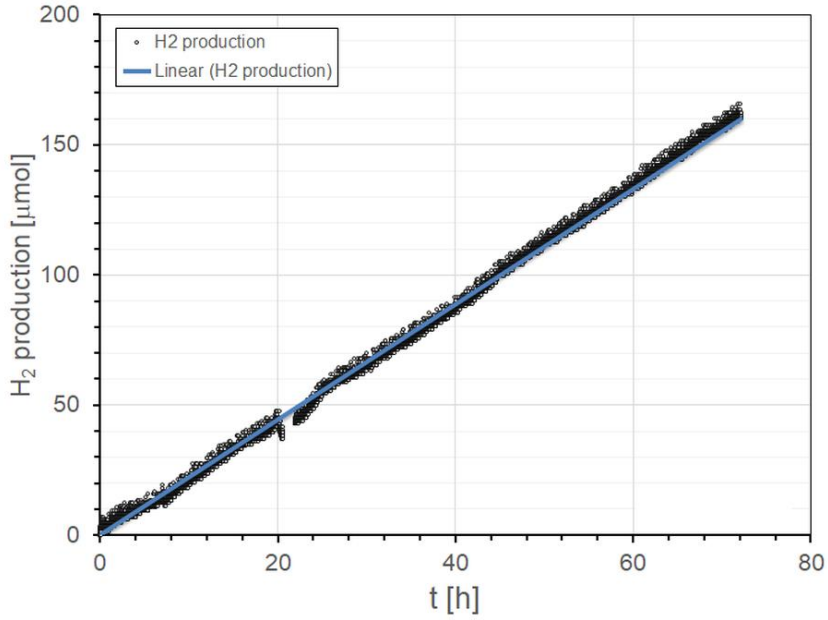

Figure 5. Photocatalytic H_2 evolution with RuNPs@CNT@mpg-CN(a) in the presence of visible light irradiation (>395 nm) from 300W Xe lamp using TEOA as the sacrificial electron donor agent with a duration of the photocatalytic reaction of 75 hrs.

3. Conclusions

Four different conducting carbon nanomaterials (CNM: 0D carbon nanohorns (CNHs), 1D single-walled carbon nanotubes (CNTs), 2D reduced graphene oxide (rGO) and 3D graphite (GP)) have been plenty decorated with Ru nanoparticles in-situ prepared through the organometallic approach resulting in four new nanohybrids generically named as RuNPs@CNM.

When physically mixed with mesoporous graphitic carbon nitride (mpg-CN) using a mortar, these novel hybrid nanomaterials highly improve the performance of bare mpg-CN as photocatalyst for the HER reaction using TEOA as sacrificial electron donor. The carbon materials furthermore provide excellent electrically conductivity between the mpg-CN and the Ru co-catalyst. Moreover, they display large surface areas and easy tunabilities, making them excellent supports for hosting RuNPs.

Initial RuNPs@CNH : mgp-CN ratio tests have shown that for high concentrations of RuNPs@CNM, the efficiency of the system as photocatalyst for the HER reaction decreases since its darkness prevents the light from reaching the photoactive surface of mpg-CN. Therefore, a compromise between two competitive effects has to be reached: i) more light is adsorbed by mpg-CN for lower RuNPs@CNM concentration, but ii) more active Ru centres are present for higher RuNPs@CNM concentration. This compromise is found for low loadings of RuNPs@CNM on the nanohybrids (0.68 and 1.69 µmol of Ru loadings). Therefore, complete photocatalytic experiments were carried out using these low Ru loadings using visible light irradiation (>395 nm) for 24 hours.

In all cases, higher amounts of H_2 has been produced with the higher loading of Ru but higher TON (considering total amount of Ru) have been obtained for the lower metal loading. More specifically, the best performance was obtained with RuNPs@CNT/mpg-CN. This system produces between 4 and 26% more H_2, and its TON is between 12 and 43% higher than for the other hybrid nanomaterials.

All in all, CNMs have proved to be an appropriate support for the stabilization of small RuNPs and also provide excellent electrical conductivity between the mpg-CN and the Ru co-catalyst. Furthermore, the use of the obtained hybrid materials in the photocatalytic HER highly improves, both in terms of activity and stability (there is no sign of deactivation for 75 h), the performance of pristine mpg-CN. Importantly, CNMs as nanotemplates to support RuNPs represent one of the few examples where RuNPs can efficiently carry out the electron-transfer process for the photocatalytic HER reaction with visible light and in absence of an electron mediator.

4. Experimental Part

4.1. General procedure and reagents

All operations for the synthesis of the materials were carried out using standard Schlenk tubes, Fischer–Porter bottle techniques or in a glovebox (MBRAUN Unilab) under argon atmosphere. The following chemicals were used as purchased: [(Ru(cod)(cot)] from NanoMePS-Toulouse, hydrogen (H_2) gas from Abelló Linde (>99,999%) and carbon nanohorns (CNH) and flaked graphite (GP) from Sigma-Aldrich. Reduced graphene oxide (rGO) was synthesized from GP following a previous methodology [30]. Raw single-walled CNTs were provided by SES Research. Mesoporous graphitic carbon nitride (mpg-CN) was synthesized in the group of Prof. Arne Thomas (TU Berlin) as described below. Tetrahydrofuran (THF) and hexane solvents, from Scharlab, were distilled and dried, and then degassed prior to their use according to a freeze–pump–thaw process.

4.2. Synthesis of mpg-CN

The mesoporous graphitic carbon nitride (mpg-CN) was synthesized via a sol-gel route according to our previously reported procedure [31] and it consists on the use of cyanamide and triethylorthosilicate as precursors to produce carbon nitride and silica mixtures. Silica is used as the template for the final mpg-CN. The removal of SiO_2 is obtained by treatment of the mixture with NH_4HF_2, yielding the desired mpg-CN.

4.3. Synthesis of carbon-supported Ru-based nanoparticles

10 mg of the selected carbon material (CNH, CNT, rGO or GP) were weighed inside a glove box and placed into a Fischer-Porter bottle together with 40 mL of THF. The reactor was placed in an ultrasonic bath for 30 min to allow the adequate dispersion of the material. It was then placed again in the glove box where [Ru(cod)(cot)] was weighed (40 mg, 0.128 mmol) and added. In this step, the reactor was pressurized with 3 bar of H_2 at room temperature and the reaction was left running for 2 h. Once the H_2 pressure was evacuated, a carbon-coated copper grid (400 mesh) for TEM analysis was prepared by adding a single drop of the colloidal solution. The carbon-supported Ru-based nanoparticles were isolated after precipitation by hexane addition and dried under vacuum.

4.4. Characterization

The crude colloidal solution has been characterized by transmission electron microscopy (TEM) and, after isolation, by inductively coupled plasma mass spectrometry (ICP-MS) and X-ray photoelectron spectroscopy (XPS). The reaction mixtures before the photocatalytic HER experiments have been characterized by Scanning Electron Microscopy-Field Emission Gun (SEM-FEG) and Energy-Dispersive X-ray spectroscopy (EDX). The reaction mixtures after performing the photocatalytic HER experiments have been characterized by transmission electron microscopy (TEM) and X-ray photoelectron spectroscopy (XPS).

4.4.1. Transmission Electron Microscopy (TEM)

TEM analyses were performed at the Servei de Microscopia de la Universitat Autònoma de Barcelona with a JEOL JEM 2010 electron microscope working at 200 kV with a resolution point of 2.5 Å. The size distributions were determined via manual analysis of enlarged micrographs, treated with ImageJ software, by measuring ca. 200 particles on a given grid to obtain a statistical size distribution and a mean diameter.

4.4.2. Inductively coupled plasma optical emission spectrometry (ICP-MS).

The real concentration (wt.%) of Ru on the as prepared photocatalyst was measured by an inductively coupled plasma optical emission spectrometry (ICP-OES) Perkin-Elmer Optima 4300DV model system located in the Chemical Analyses Service of the Universitat Autònoma de Barcelona.

4.4.3. X-ray Photoelectron Spectroscopy (XPS)

The chemical composition of the photocatalysts were investigated using X-ray Photoelectron Spectroscopy which was performed with a Phoibos 150 analyzer (SPECS GmbH, Berlin, Germany) in ultra-high vacuum conditions (base pressure $5 \cdot 10^{-10}$ mbar) with a monochromatic aluminium Kalpha x-ray source (1486.74 eV). The energy resolution measured by the FWHM of the Ag $3d^{5/2}$ peak for a sputtered silver foil was 0.62 eV. located at Catalan Institute of Nanoscience and Nanotechnology (ICN2) in Barcelona.

4.4.4. Scanning Electron Microscopy-Field Emission Gun (SEM-FEG) and Energy-Dispersive X-ray spectroscopy (EDX)

Scanning Electron Microscopy-Field Emission Gun (SEM-FEG) and Energy-dispersive X-Ray Spectroscopy (EDX) analyses were performed at the Servei de

Microscopia de la UAB using a JEOL JSM 6700F electron microscope working at 10 kV.

4.4.5. Specific Surface Area (S_{BET})

The surface area was measured on a Quantachrome Autosorb-1 apparatus. Nitrogen adsorption–desorption isotherms were measured at 77.350 K after degassing the samples at 120 °C for 6 h. The BET surface areas (SBET) were calculated from the adsorption data in a relative pressure region of 0.05 to 1 bar.

4.4.6. X-ray Powder Diffraction (XRD)

The XRD patterns were measured in Bruker AXS D8 advanced diffractometer equipped with a position sensitive detector (PSD) and a curved germanium (111) primary monochromator and the radiation used was Cu-Kα (λ =1.5418 Å).

4.5. Photocatalytic tests

4.5.1. Photocatalytic tests in screening reactor.

26.3 mg of mpg-CN together with the corresponding amount of RuNPs@CNT were placed into the glass reactor (total volume of the reactor 35 mL, see Figure S7 in Supporting Information). Then, 20 mL of an aqueous solution with 10 vol.% triethanolamine as the sacrificial reagent were added into the reactor cell. The reaction mixture was rinsed with argon for 10 minutes. The reactor was closed with a septum and then irradiated with the Xenon lamp (L.O.T. Oriel QuantumDesign, Germany with a 395 nm filter) for 4 hrs. The distance from the lamp to the reactor was 10 cm and the reactor was cooled to 19°C using a thermostat (Huber, ministat 125). Then, 8 mL of the gas in the headspace was taken with a syringe, which had been previously flushed with argon. The hydrogen content in the gas volume was measured with two injections of 4 mL each in a gas chromatograph.

4.5.2. Photocatalytic tests in standard reactor.

25 mg of mpg-CN together with the corresponding amount of RuNPs@CNT were placed into the reactor (total volume of the reactor 51.3 mL; see Figures S9 and S10 for the experimental setup and a schematic drawing of the reactor, respectively, in the Supporting Information). The reactor was then sealed with a quartz glass. The reactor is connected to a Schlenk-Line apparatus (argon/vacuum). After the reactor was evacuated, 38 mL of an aqueous solution with 10 vol.%

triethanolamine as the sacrificial reagent, which was previously flushed with argon for 20 minutes, was added with a syringe through a tap at the head of the reactor with an argon counter current. The reaction mixture was irradiated with a Xenon lamp (L.O.T. Oriel QuantumDesign, Germany, with a 395 nm filter) under constant stirring for 24 hrs. The temperature was constant at 30°C by using a thermostat (LAUDA ECO RE 630). The distance from the lamp to the reactor was 10 cm. The pressure curve in the reactor was measured with a pressure sensor (Type-P30, $\Delta p = \pm 0.1$, WIKA Alexander Wiegand SE & Co. KG, Germany). At a constant temperature of the reaction mixture, the amount of hydrogen produced can be determined with the ideal gas equation.

In addition, the hydrogen content was determined by gas chromatography. For that, 8 mL of the gas in the headspace was taken with a syringe, which had been previously flushed with argon. The hydrogen content in the gas volume was measured with two injections of 4 mL each in a gas chromatograph.

4.5.3. Gas chromatography

The amount of H_2 was determined by a gas chromatograph (GC Agilent 7890 A) equipped with a Thermal Conductivity Detector (TCD). The gas sample was manually injected into the gas chromatograph. The column in the GC consists of Carboxen 1000 and argon was used as the carrier gas.

Acknowledgements

This project was funded by the Federal Ministry of Education and Research of Germany under the ”CO_2Plus funding measure – Use of CO_2 to broaden the raw material basis” under the grant number 033RC003, by the International Postdoc Initiative (IPODI) of the European Union, and by the Deutsche Forschungsgemeinschaft (DFG, German Research Foundation) under Germany´s Excellence Strategy – EXC 2008 – 390540038" – UniSysCat and by Spanish MINECO (CTQ2015-64261-R and PID2019-104171RB-I00) . I A.-P. acknowledges the *Universitat Autònoma de Barcelona* for his pre-doctoral grant. J.G.-A. acknowledges Serra Húnter Program. The authors thank the Microscopy Service of the *Universitat Autònoma de Barcelona* for technical assistance with TEM and SEM.

References

[1] N. S. Lewis, *Science* 351 (2016)353.
[2] J. Qi, W. Zhang, R. Cao, Adv. Energy Mater. 8 (2018) 17018620.
[3] M. P. Browne, J. Plutnar, A. M. Pourrahimi, Z. Sofer, M. Pumera, *Adv. Energy Mat.* 9 (2019) 1900994.
[4] T. Hisatomi, J. Kubota, K. Domen, *Chem. Soc. Rev.* 43 (2014) 7520 – 7535.
[5] A. Eftekhari, *Int. J. Hydrogen Energy* 42 (2017) 11053 – 11077.
[6] A. Barrozo, M. Orio, *ChemSusChem* 12 (2019) 4905 – 4915.
[7] A. Fujishima, K. Honda, *Nature* 238 (1972) 37 – 38.
[8] J. Zhu, L. Hu, P. Zhao, L. Y. Suk Lee, K.-Y. Wong, *Chem. Rev.* 120 (2020) 851 – 918.
[9] K. Philippot, P. Serp, In Nanomaterials in Catalysis; Serp, P., Philippot, K., Eds.; Wiley-VCH: Weinheim, 2013; Chapter 1, pp 1−54.
[10] J. Creus, J. De Tovar, N. Romero, J. García-Antón, K. Philippot, R. Bofill, X. Sala, *ChemSusChem* 12 (2019) 2493 – 2514.
[11] J. Yu, Q. He, G. Yang, W. Zhou, Z. Shao, M. Ni, *ACS Catal.* 9 (2019) 9973 – 10011
[12] S. Han, Q. Yun, S. Tu, L. Zhu, W. Cao, Q. Lu, *J. Mater. Chem. A.* 7 (2019) 24691 – 24714.
[13] S. Fukuzumi, Y. Yamada, *J. Mater. Chem.* 22 (2012) 24284–24296.
[14] Y. Yamada, S. Shikano, S. Fukuzumi, *J. Phys. Chem. C* 117 (2013) 13143–13152
[15] Y. Yamada, T. Miyahigashi, H. Kotani, K. Okubo, S. Fukuzumi, *J. Am. Chem. Soc.* 113 (2011) 16136–16145.
[16] Y. Yamada, T. Miyahigashi, K. Ohkubo, S. Fukuzumi, *Phys. Chem. Chem. Phys.* 14 (2012) 10564–10571.
[17] C. Amiens, B. Chaudret, D. Ciuculescu-Pradines, V. Collière, K. Fajerwerg, P. Fau, M. Kahn, A. Maisonnat, K. Soulantica, K. Philippot, *New J. Chem.* 37 (2013) 3374 − 3401.
[18] C. Amiens, D. Ciuculescu-Pradines, K. Philippot, *Coord. Chem. Rev.* 308 (2016) 409 − 432.
[19] S. Drouet, J. Creus, V. Collière, C. Amiens, J. García-Antón, X. Sala, K. Philippot, *Chem. Commun.* 53 (2017) 11713 – 11716.
[20] J. Creus, S. Drouet, S. Suriñach, P. Lecante, V. Colliere, R. Poteau, K. Philippot, J. García-Antón, X. Sala, *ACS Catal.* 8 (2018) 11094 – 11102.
[21] J. Creus, L. Mallón, N. Romero, R. Bofill, A. Moya, J. L. G. Fierro, R. Mas-Ballesté, X. Sala, K. Philippot, J. García-Antón, *Eur. J. Inorg. Chem.* (2019) 2071 – 2077.
[22] Y. Zheng, J. Liu, J. Liang, M. Jaroniec, S. Z. Qiao, *Energy Environ. Sci.* 5 (2012) 6717 – 6731.
[23] Y. Zheng, L. Lin, B. Wang, X. Wang, *Angew. Chem. Int. Ed.* 54 (2015) 12868 – 12884.
[24] J. Zhang, Y. Chen, X. Wang, *Energy Environ. Sci.* 8 (2015) 3092 – 3108.
[25] G. Zhang, G. Li, T. Heil, S. Zafeiratos, F. Lai, A. Savateev, M. Antonietti, X. Wang, *Angew. Chem. Int. Ed.* 58 (2019) 3433-3437.
[26] A. Savateev, Z. P. Chen, D. Dontsova, *RSC Adv.* 6 (2016) 2910-2913.
[27] Y. Wang, Y. Li, S. Cao, J. Yu, *Chinese J. Catal.* 40 (2019) 867-874.
[28] J. García-Antón, M.R. Axet, S. Jansat, K. Philippot, B. Chaudret, T. Pery, G. Buntkowsky, H.-H. Limbach, *Angew. Chem. Int. Ed.* 47 (2008) 2074 – 2078.
[29] M. Tasbihi, A. Acharjya, A. Thomas, M. Reli, N. Ambrozova, K. Kocl, R. Schomäcker, *J. Nanosc. Nanotech.* 18 (2018) 5636-5644.
[30] J. Muñoz, L. J. Brennan, F. Céspedes, Y. K. Gun'ko, M. Baeza, *Comp. Sci. Tech.* 125 (2016) 71 – 79.
[31] K. Kailasam, J. D. Epping, A. Thomas, S. Losse, H. Junge, *Energy Environ. Sci.* 4 (2011) 4668 – 4674.